Developmental Biology 401 (2015) 236–248

Contents lists available at ScienceDirect

Developmental Biology

journal homepage: www.elsevier.com/locate/developmentalbiology

Claudin-10 is required for relay of left–right patterning cues from Hensen's node to the lateral plate mesoderm

Michelle M. Collins [a,c], Amanda I. Baumholtz [a,c], Annie Simard [c], Mary Gregory [d], Daniel G. Cyr [a], Aimee K. Ryan [a,b,c,*]

[a] Departments of Human Genetics, McGill University, Canada
[b] Departments of Paediatrics, McGill University, Canada
[c] The Research Institute of the McGill University Health Centre, Montréal, Québec, Canada
[d] INRS-Institut Armand Frappier, Laval, Québec, Canada

ARTICLE INFO

Article history:
Received 19 July 2014
Received in revised form
19 February 2015
Accepted 23 February 2015
Available online 3 March 2015

Keywords:
Left–right patterning
Claudins
Tight junctions
Chick development
Claudin-10
Nodal
Pitx2c
Heart tube looping
Asymmetry
Laterality cues
Hensen's node
Lateral plate mesoderm

ABSTRACT

Species-specific symmetry-breaking events at the left–right organizer (LRO) drive an evolutionarily-conserved cascade of gene expression in the lateral plate mesoderm that is required for the asymmetric positioning of organs within the body cavity. The mechanisms underlying the transfer of the left and right laterality information from the LRO to the lateral plate mesoderm are poorly understood. Here, we investigate the role of Claudin-10, a tight junction protein, in facilitating the transfer of left–right identity from the LRO to the lateral plate mesoderm. Claudin-10 is asymmetrically expressed on the right side of the chick LRO, Hensen's node. Gain- and loss-of-function studies demonstrated that right-sided expression of Claudin-10 is essential for normal rightward heart tube looping, the first morphological asymmetry during organogenesis. Manipulation of Claudin-10 expression did not perturb asymmetric gene expression at Hensen's node, but did disrupt asymmetric gene expression in the lateral plate mesoderm. Bilateral expression of Claudin-10 at Hensen's node prevented expression of *Nodal*, *Lefty-2* and *Pitx2c* in the left lateral plate mesoderm, while morpholino knockdown of Claudin-10 inhibited expression of *Snail1* in the right lateral plate mesoderm. We also determined that amino acids that are predicted to affect ion selectivity and protein interactions that bridge Claudin-10 to the actin cytoskeleton were essential for its left–right patterning function. Collectively, our data demonstrate a novel role for Claudin-10 during the transmission of laterality information from Hensen's node to both the left and right sides of the embryo and demonstrate that tight junctions have a critical role during the relay of left–right patterning cues from Hensen's node to the lateral plate mesoderm.

Introduction

In vertebrates, organs are positioned asymmetrically within the body cavity. This allows for efficient packaging of organs and their associated vasculature in a limited space and is required for normal organ physiology. The molecular cascade that patterns the left–right axis initiates at gastrulation. Although the events that initiate symmetry breakage at the left–right organizer (LRO) are species-specific, they lead to an evolutionarily-conserved cascade of asymmetric gene expression in the lateral plate mesoderm. The mechanisms that drive the transmission of laterality cues from the site of symmetry breaking to the lateral plate mesoderm are not well understood. Recent work in the mouse has pointed to a role for the endoderm in the relay of these signals (Saund et al., 2012; Viotti et al., 2012), but a similar mechanism has yet to be identified in the chick.

In the chick, several mechanisms are required to break symmetry at Hensen's node, including the left-sided flux of intracellular and extracellular calcium ions (Raya et al., 2004; Garic-Stankovic et al., 2008), the leftward movement of cells at Hensen's node (Cui et al., 2009; Gros et al., 2009), membrane depolarization along the primitive streak via ion pumps (Levin and Mercola, 1998; Aw et al., 2008; Aw et al., 2010), and movement of small molecules, such as the neurotransmitter serotonin, through gap junctions (Fukumoto et al., 2005a, 2005b; Adams et al., 2006). These events culminate in the restriction of *Shh* expression to the left side of Hensen's node at HH4^{+} due to inhibition of its expression on the right side by BMP signalling. SHH signalling then induces *Nodal* expression in the left perinodal region, and subsequently in the left lateral plate mesoderm. Lateral plate mesoderm expression of Nodal is modulated by different levels of BMP signalling via the Cerberus/Dan family of BMP antagonists

* Corresponding author.
E-mail address: aimee.ryan@mcgill.ca (A.K. Ryan).

http://dx.doi.org/10.1016/j.ydbio.2015.02.019
0012-1606/

and SMAD effectors (Katsu et al., 2012, 2013). Additionally, *Nodal* expression is attenuated via a negative regulatory feedback loop with Lefty1 in the midline and Lefty2 in left lateral plate mesoderm (reviewed in Shen, 2007). Nodal signalling activates expression of the homeodomain transcription factor *Pitx2c* in the left lateral plate mesoderm, which is subsequently expressed on the left side of organs that are undergoing asymmetric morphogenesis and/or positioning (reviewed in Nakamura and Hamada, 2012). The Nodal-Pitx2c cassette is evolutionarily conserved in all vertebrates, as well as in some invertebrates (Okumura et al., 2008; Grande and Patel, 2009; Grande, 2010; Luo and Su, 2012; Nakamura and Hamada, 2012). Asymmetric gene expression and signalling is also important on the right side of Hensen's node. Early asymmetries in activin signalling induce right-sided BMP signalling that represses *Shh* expression on the right and subsequently activates expression of FGF8 in the right perinodal region. FGF8 in turn induces expression of *Snail1* (*cSnR1*) in the right lateral plate mesoderm (Boettger et al., 1999). Negative reciprocal interactions between signalling molecules and the midline barrier compartmentalize the signalling cascades to the left and right sides of the embryo.

Tight junctions function apically within the plasma membrane where they regulate the movement of ions and small molecules through the paracellular space, contribute to polarity by restricting mixing of the apical and basolateral membrane components, and play a role in cell–cell adhesion (reviewed in Gonzalez-Mariscal et al., 2003; Gupta and Ryan, 2010; Steed et al., 2010). Claudins oligomerize to form the strands of tight junctions and the specific properties of the tight junction are determined by the subset of claudin family members present. A role for claudins and tight junctions in asymmetric morphogenesis appears to be conserved. We previously showed in the chick that overexpression of the tight junction protein Claudin-1 on the right side of Hensen's node randomizes the direction of heart-looping (Simard et al., 2006). In *Xenopus*, overexpression of the claudin *Xcla* at the four-cell stage randomizes organ situs (Brizuela et al., 2001), and alterations in tight junction regulation downstream of the potassium ATP channel (K_{ATP} channel) have been reported to disrupt left–right patterning in both the chick and in *Xenopus* (Aw et al., 2010). Furthermore, the *C. elegans* claudin superfamily member *nsy-4* also has a role in generating left–right asymmetry in olfactory neurons (Vanhoven et al., 2006).

The Claudin-1 knock-out mouse does not have left–right patterning defects (Furuse et al. 2002), which led us to speculate that the induction of leftward heart looping following overexpression of Claudin-1 on the right side could be due to its ability to antagonize the function of another family member. Therefore, we investigated if additional members of the claudin family of integral tight junction proteins are required for normal left–right patterning in chick embryos. Our analysis of the expression patterns of 17 claudin family members in the chick embryo revealed that *Claudin-10* is asymmetrically expressed on the right side of Hensen's node (Collins et al., 2013). Here, we report that alteration of the *Claudin-10* asymmetric expression pattern disrupted

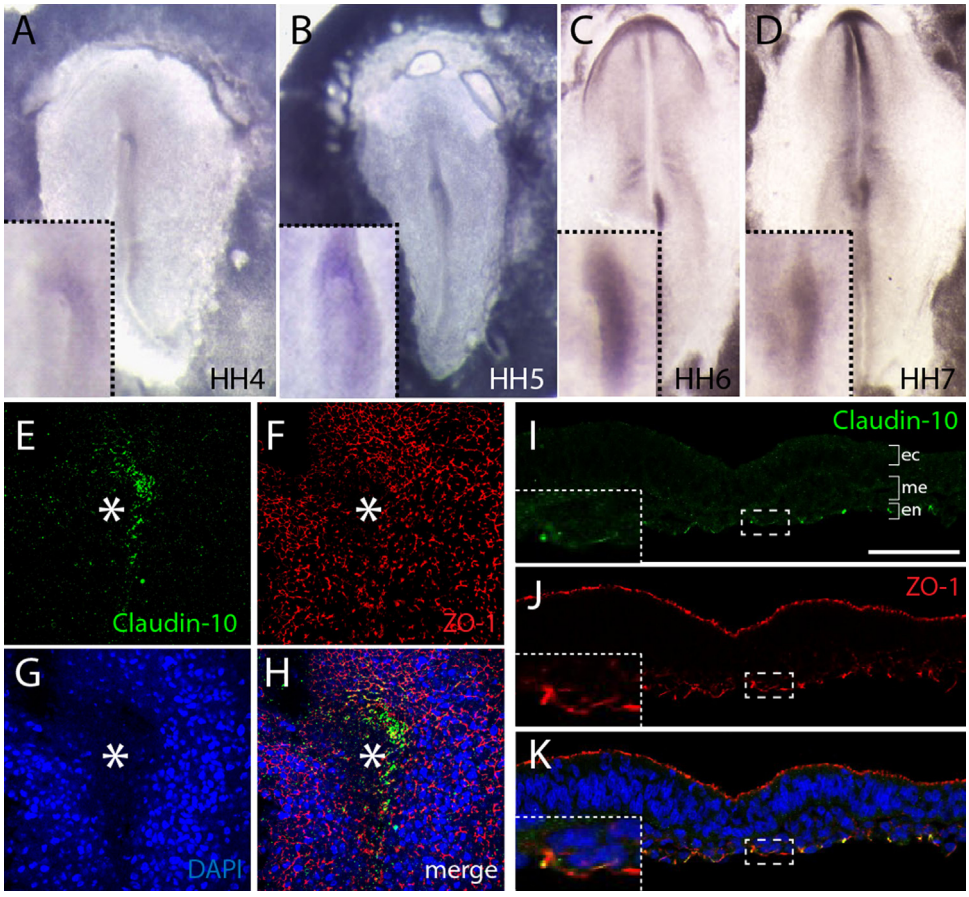

Fig. 1. *Claudin-10 is asymmetrically expressed on the right side of Hensen's node.* (A–D) Whole-mount *in situ* hybridization was used to analyse *Claudin-10* expression. *Claudin-10* mRNA is faintly detected at HH4 (A) and becomes asymmetrically expressed on the right side of Hensen's node by HH4^{+} until HH7 (B–D). Higher magnifications of Hensen's node are shown in the inset (outlined by dashed line). (E–H) Dorsal views of a HH5 embryo subjected to whole-mount immunohistochemistry. Claudin-10 (green; E) is localized to the right side of Hensen's node (*) where it colocalizes with ZO-1 (red; F). DAPI (blue) was used to stain the nuclei (G). (I–K) Immunohistochemistry showing Claudin-10 and ZO-1 expression in sections from a HH5 embryo. Higher magnifications of endodermal cells are shown in the inset (outlined by white dashed box and line). All embryos are shown as dorsal views. Abbreviations: ec, ectoderm; me, mesoderm; en, endoderm. Scale bar in I represents 100 μm.

expression of asymmetrically expressed genes in the midline and lateral plate mesoderm, and randomized the direction of heart-looping, the earliest morphological asymmetry in the embryo. Using a mutagenesis approach, we identified critical amino acids in two functional domains that are required for Claudin-10 to function in left–right patterning: D73, located in the first extracellular loop, which determines ion selectivity of the tight junction, and S218 and the PDZ-binding domain in the cytoplasmic tail, which participates in protein interactions that link the apical tight junction to the actin cytoskeleton. Finally, we assessed cell polarity in Claudin-10 morphant embryos and observed that actin organization and apical-basal polarity was unaffected. This is the first report of a role for Claudin-10 in asymmetric morphogenesis and suggests a novel function for tight junctions in the relay of laterality cues from Hensen's node to the lateral plate mesoderm.

Results

Claudin-10 is asymmetrically expressed at Hensen's node

We previously investigated the expression patterns of 17 chick claudin family members and found that *Claudin-10* was asymmetrically expressed on the right side of Hensen's node at HH5 (Collins et al., 2013). Here, we extended this analysis to more precisely define the duration and location of *Claudin-10* expression. Whole-mount *in situ* hybridization revealed that *Claudin-10* was present at Hensen's node at HH4, and its expression became strongly asymmetric on the right side of the node from HH4^{+} to HH7 (Fig. 1A–D). Expression was dramatically decreased at HH8. Significant levels of *Claudin-10* expression were not observed elsewhere in the embryo until the emergence of the pronephros at HH18, as we previously reported (Collins et al., 2013). Immunohistochemistry was performed on whole embryos and sections to determine the cellular localization of Claudin-10 (Fig. 1E–K). Confocal projections of the whole embryo revealed that Claudin-10 protein was symmetrically localized at HH4 and then became localized to a discrete region on the right side of the inner curvature of Hensen's node that corresponded to the *Claudin-10* expression domain observed by *in situ* hybridization (Fig. 1E–H; Supplemental Fig. 1). Claudin-10 expression extended posteriorly from Hensen's node along the right side of the anterior-most region of the primitive streak (Fig. 1E and H). To confirm that this signal was not an artifact, we performed whole mount immunohistochemistry to analyse expression of another claudin family member, Claudin-1, and the tight junction cytoplasmic adaptor protein ZO-1. We have previously shown that Claudin-1 is expressed uniformly in the ectoderm at early stages of chick embryogenesis (Simard et al., 2006). Whole-mount immunofluorescence showed that both Claudin-1 and ZO-1 were uniformly expressed in the ectoderm on both the left and right sides of the embryo. Claudin-1 expression was highest in the cells immediately surrounding the node but again there were no apparent asymmetries in Claudin-1 expression (Fig. 1F, Supplemental Fig. 1). Analysis of sections from HH5 embryos showed that Claudin-10 colocalized with the tight junction marker ZO-1 in a punctate pattern at the apical surface of the endoderm underlying Hensen's node (Fig. 1I–K). Claudin-10 mRNA and protein were never detected in the lateral plate mesoderm nor in the developing heart tube.

Manipulating Claudin-10 expression randomizes the direction of heart looping

Based on the spatial and temporal aspects of *Claudin-10* expression, we hypothesized that asymmetric Claudin-10 is required on the right side of Hensen's node for patterning the left–right axis of the developing embryo. We performed gain- and loss-of-function experiments to generate bilateral and absent Claudin-10 expression, respectively, and used the direction of heart tube looping as a morphological read-out for the effects of these manipulations on left–right patterning. To define the developmental window during which Claudin-10 exerts its effect on the left–right patterning cascade, we performed these manipulations between HH4 and HH7, when asymmetric expression of *Claudin-10* is observed. Embryos were collected at HH3, cultured until they reached the appropriate stage, and then injected with retrovirus or electroporated with a morpholino.

Bilateral Claudin-10 expression randomizes the direction of heart tube looping

To generate bilateral expression of Claudin-10, we injected control RCAS-GFP or RCAS-Claudin-10 retroviral particles on the left side of Hensen's node (Fig. 2A and B) at HH3-4. A significant increase in the incidence of abnormal leftward heart tube looping was observed following Claudin-10 misexpression (30.6%, $n=59/193$, $\chi^2=20.85$, $p<0.0001$) versus injection of the GFP control virus (10.6%, $n=17/161$) (Fig. 2G). Retroviral misexpression of Claudin-10 on the left side of Hensen's node at HH5 also caused an increase in abnormal leftward heart tube looping (23.9%; $n=17/71$) compared to the GFP control (14.3%, $n=3/21$), although this effect did not reach significance ($\chi^2=0.89$, $p=0.30$). Injection of Claudin-10 retroviral particles at HH6 or HH7 did not affect the direction of heart tube looping (Fig. 2G).

To determine the effect of overexpressing Claudin-10 on the right side of Hensen's node where it is endogenously expressed, we injected Claudin-10 virus or a GFP control virus at HH4. Neither Claudin-10 nor GFP virus altered the direction of heart tube looping when injected on the right side of the embryo (Fig. 2G) when compared to the levels of leftward heart tube looping observed previously by our group and others following *ex ovo* culture of chick embryos (Katsu et al., 2012; Simard et al., 2006; Yu et al., 2001). These data suggest that Claudin-10 must be asymmetrically expressed on the right side of the embryo for correct left–right patterning.

Claudin-10 knockdown randomizes the direction of heart tube looping

To determine if Claudin-10 is essential for normal rightward looping of the heart tube, we used a fluorescein-tagged antisense morpholino (MO) that targets the ATG start site of the *Claudin-10* transcript to specifically knockdown endogenous Claudin-10 expression at Hensen's node. Embryos were electroporated with either the *Claudin-10* MO or a 5 base pair mismatch control MO at HH3-4. Immediately following electroporation, cells that had incorporated the fluorescein-tagged morpholinos were observed surrounding Hensen's node (Fig. 2C and C'). The embryos were scored for the direction of heart tube looping 24 h after electroporation (Fig. 2D and E), at which time the majority of the fluorescein-positive cells were detected along the midline (Fig. 2D' and E') and endogenous Claudin-10 protein was markedly reduced (Fig. 2F). Greater than 90% of the electroporated embryos exhibited normal development along the anterior–posterior axis and had no gross morphological defects. The *Claudin-10* mismatch MO had no effect on the direction of heart tube looping; abnormal leftward looped heart tubes were observed in less than 10% ($n=9/96$) of the embryos. In contrast, 50% of the embryos electroporated with the *Claudin-10* MO exhibited an abnormal leftward looped heart tube ($n=58/117$, $\chi^2=39.52$, $p<0.0001$) (Fig. 2H). These data demonstrate that Claudin-10 is required for normal rightward looping of the heart tube.

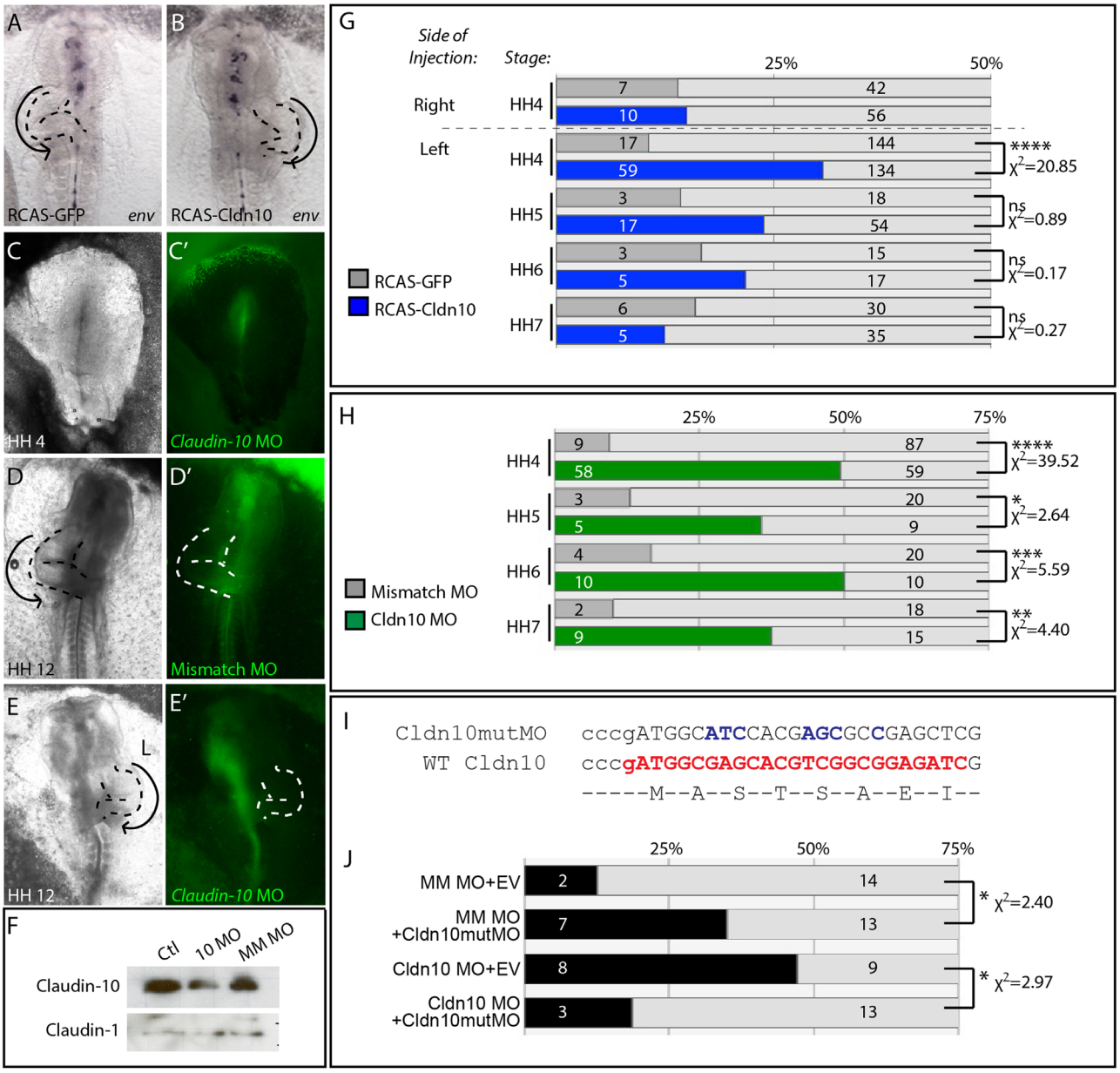

Fig. 2. *Asymmetric expression of Claudin-10 is required for normal heart tube morphogenesis.* (A and B) Gain-of-function experiments were performed using retroviral particles encoding Claudin-10 or GFP as a control. Embryos stained using an antisense *RCAS env* riboprobe show that RCAS-infected cells are found along the midline of the embryo. Ventral views of embryos showing a normal rightwardly looped heart tube (A) and an abnormal leftwardly looped heart tube (B). (C–E) Loss-of-function experiments were performed by electroporation of a fluorescein-tagged morpholino (MO) against *Claudin-10*, using a mismatch MO as control. (C and C') Ventral view of a HH4 embryo electroporated with *Claudin-10* MO showing fluorescein-positive cells at Hensen's node and along the primitive streak. (D) Ventral view of a HH12 embryo electroporated with a mismatch control MO showing a normal rightward looping heart tube. (E) Ventral view of a HH12 embryo electroporated with a *Claudin-10* MO showing an abnormal leftward looping heart tube. (D' and E') Electroporated cells are apparent along the midline of the embryo. (F) Western blot showing the relative levels of Claudin-10 protein in a pool of HH12 embryos electroporated with either the *Claudin-10* MO (10 MO) or mismatch control MO (MM MO), or uninjected controls (Ctl). The blot was stripped and reprobed with an antibody against Claudin-1. (G) Heart tube looping scores for RCAS-GFP and RCAS-Claudin-10 injections on the right or left side of the embryo between HH4 and HH7. Dark grey and blue bars indicate the number of abnormal leftward looped heart tubes for control and RCAS-Claudin10, respectively. Light grey bars indicate the number of normal rightward looped heart tubes. (H) Heart tube looping scores for *Claudin-10* and mismatch morphant embryos electroporated at the stages indicated. Dark grey and green bars indicate the number of abnormal leftward looped heart tubes for control mismatch morpholino and Claudin-10 morphants, respectively. Light grey bars indicate the number of normal rightward looped heart tubes. (I and J) Morpholino rescue experiment. (I) Schematic of Cldn10mutMO binding site of morpholino (shown in red) and mutated nucleotides (shown in blue). (J) Heart tube looping scores for embryos electroporated with the indicated combination of morpholino and expression vectors. EV indicates empty vector control. ns=non-significant, *$p<0.05$, **$p<0.01$, ***$p<0.001$, ***$p<0.0001$.

Morpholinos electroporated at HH3-4 are predicted to block Claudin-10 protein expression at Hensen's node between stages HH4 and HH8 due to the stability of the morpholino. To more precisely map the temporal window of Claudin-10 function during the establishment of left–right patterning, we electroporated *Claudin-10* morpholinos at later timepoints (Fig. 2H). Following electroporation at HH5, *Claudin-10* morphants showed a 36% ($n=5/14$) incidence of leftward heart tube looping as compared to a 13% incidence in embryos injected with the mismatch control MO ($\chi^2=2.64$, $p=0.04$). Electroporation at HH6 caused 50% ($n=10/20$) of *Claudin-10* morphants to have abnormal leftward looped heart tubes as compared to 17% of control embryos ($\chi^2=5.59$, $p=0.01$). Finally at HH7, 38% ($n=9/24$) of *Claudin-10* morphant embryos had abnormal leftward heart tube looping as compared to the 10% of control embryos ($\chi^2=4.4$, $p=0.03$) (Fig. 2H).

To confirm that these phenotypes were specific to knockdown of Claudin-10, we performed rescue experiments by co-electroporation of the morpholinos with either an empty expression vector or one that expressed a variant *Claudin-10* transcript (Cldn10mutMO) that could not be recognized by the *Claudin-10* morpholino (Fig. 2I and J). Embryos electroporated with the mismatch MO and empty vector (EV) had a background incidence of leftward looped hearts tubes (12.5%; $n=2/16$). In contrast, 35% ($n=7/20$) of embryos electroporated with the *Claudin-10* mismatch MO and pMES-Cldn10mutMO had leftward looped heart tubes (Fig. 2H). This effect is similar to what we observed when Claudin-10 was retrovirally misexpressed on the left side of the embryo, supporting that the *Cldn10mutMO* transcript encodes a fully functional Claudin-10 protein as predicted. Embryos electroporated with the *Claudin-10* MO and empty vector had a 53% ($n=9/17$) incidence of leftward looping heart tubes, similar to the incidence observed with *Claudin-10* MO alone (Fig. 2J). This phenotype was rescued by co-electroporation of the *Claudin-10* MO with the pMES-Cldn10mutMO construct (18% leftward heart looping; $n=3/16$). The ability of the morpholino-insensitive Claudin-10 construct to rescue the laterality phenotype indicates that the *Claudin-10* MO is specifically targeting *Claudin-10* transcripts.

Manipulation of Claudin-10 expression does not affect asymmetric gene expression at Hensen's node

Our gain- and loss-of-function experiments clearly demonstrated that asymmetric expression of Claudin-10 the right side of Hensen's node is essential for the initiation of asymmetric heart morphogenesis. To determine where Claudin-10 functions within the cascade of left–right patterning cues, we investigated the effects of manipulating Claudin-10 expression on the asymmetric expression of left–right patterning genes. Following retroviral injection or morpholino electroporation at HH3, embryos were collected at HH5 to analyse *Shh* and *Fgf8* expression on the left and right sides of Hensen's node, respectively, or at HH6-HH8 to analyse expression of *Nodal* in the left perinodal region by whole-mount *in situ* hybridization. Additionally, a subset of embryos from each manipulated group was left until HH12 to score the direction of heart tube looping.

Asymmetric expression of *Shh* on the left side of Hensen's node and *Fgf8* on the right side immediately precede asymmetric expression of *Claudin-10* on the right. In addition, our gain- and loss-of-function experiments place Claudin-10 function temporally downstream of Shh and Fgf8 function in asymmetric morphogenesis. Therefore, we predicted that their expression patterns would be unchanged in our Claudin-10 manipulated embryos. Indeed, normal expression of *Fgf8* ($n=10$) and *Shh* ($n=14$) on the right and left sides of Hensen's node, respectively, were observed in gain-of-function embryos that express bilateral Claudin-10 (Supplemental Fig. 2). Expression patterns of *Fgf8* ($n=9$) and *Shh* ($n=10$) were also unaffected in the *Claudin-10* morphant embryos (Supplemental Fig. 2). In addition, all manipulated embryos exhibited normal left-sided perinodal *Nodal* expression (Fig. 3A–C).

Left-sided Claudin-10 misexpression affects left-sided gene expression

Asymmetric gene expression in the midline and the lateral plate mesoderm is evolutionarily conserved and occurs between HH6 and HH12 in the chick embryos, temporally downstream of when Claudin-10 appears to function in left–right patterning. To determine if bilateral expression of Claudin-10 disrupted these

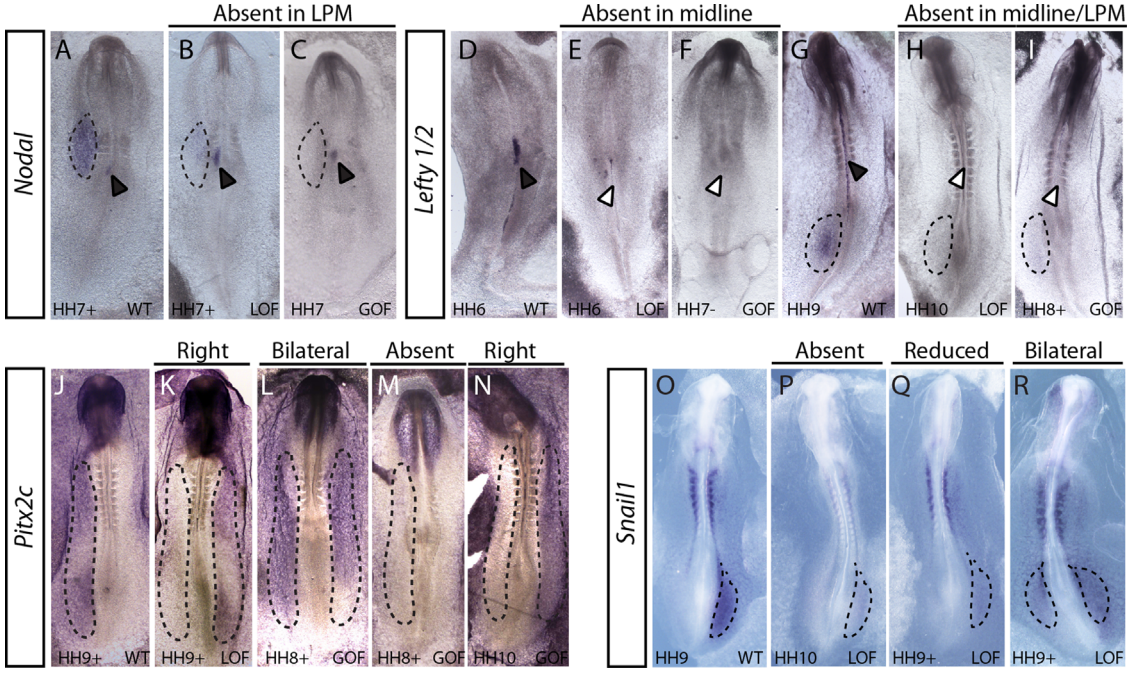

Fig. 3. *Manipulation of Claudin-10 affects Nodal, Lefty1, Lefty2, Pitx2c, and Snail1 expression.* Whole-mount *in situ* hybridization was used to examine gene expression patterns in control and Claudin-10 manipulated embryos. Dorsal views of wildtype control embryos (WT) with normal expression patterns and representative Claudin-10 gain- (GOF) and loss-of-function (LOF) embryos with disrupted gene expression patterns are shown. (A–C) Expression of *Nodal*. Panels B and C show embryos with normal left-sided perinodal expression (black arrowhead) but absent expression in the left lateral plate mesoderm (dashed outline). (D–I) Expression of *Lefty1* and *Lefty2*. Wildtype expression of *Lefty1* in the midline (black arrowhead) is shown in D, and *Lefty2* in the lateral plate mesoderm (dashed outline) in G. Panels E and F show embryos that lack *Lefty1* expression in the midline at HH6-7 (white arrowhead), and panels H and I show embryos with absent expression in both the midline (white arrowhead) and left lateral plate mesoderm (dashed outline). (J–N) Expression of *Pitx2c*. Wildtype *Pitx2c* expression in the left lateral plate mesoderm (dashed outline) of control embryos is shown in panel J. Panel K shows right-sided expression observed in morphant embryos. Examples of disrupted *Pitx2c* expression patterns in gain-of-function embryos are shown in panels L (bilateral), M (absent), and N (right-sided). (O–R) Expression of *Snail1*. Wildtype expression of *Snail1* is shown in the right lateral plate mesoderm (dashed outline) in panel O. Examples of disrupted *Snail1* expression observed in morphant embryos are shown in panels P (absent *Snail1* expression), Q (reduced *Snail1* expression), and R (bilateral *Snail1* expression).

expression patterns, we injected HH3-4 embryos with Claudin-10 retroviral particles on the left side to generate bilateral Claudin-10 expression at Hensen's node. Embryos were collected at HH6-8 to examine *Nodal* expression in the lateral plate mesoderm and *Lefty1* in the midline, or at stages HH8$^+$–HH10 to analyse expression of *Lefty2*, *Pitx2c*, and *Snail1* in the lateral plate mesoderm. All control embryos injected with the GFP retroviral particles exhibited normal left-sided expression patterns for *Lefty1*, *Nodal*, *Lefty2*, *Pitx2c*, and right-sided expression for *Snail1* (Fig. 3, Table 1). However, expression of the four genes that are asymmetrically expressed on the left side of the embryo was disrupted in gain-of-function embryos that express Claudin-10 bilaterally. *Lefty1* expression in the midline was absent in 30% ($n=3/10$) of manipulated embryos (Fig. 3F), and approximately 40% of the embryos exhibited absent *Nodal* ($n=4/10$) and *Lefty2* ($n=3/7$) expression in the left lateral plate mesoderm (Fig. 3C and I). *Pitx2c* expression was randomized in 17% of the manipulated embryos (Fig. 3L–N). As expected, asymmetric *Snail1* expression in the right lateral plate mesoderm was not affected when Claudin-10 was misexpressed on the left side of the embryo (data not shown). These data are summarized in Table 1. These data suggest that endogenous Claudin-10 expression promotes right-sided patterns of gene expression in the midline and lateral plate mesoderm by preventing the expression of left-sided genes.

Claudin-10 knockdown disrupts gene expression in both the left and right lateral plate mesoderm

To test our hypothesis that Claudin-10 expression is required for right-sided gene expression in the lateral plate mesoderm, we electroporated HH3-4 embryos with either the mismatch control or *Claudin-10* morpholino. Gene expression patterns were not affected in embryos electroporated with the mismatch control morpholino. In support of our hypothesis, *Snail1* expression was disrupted in 49% of the *Claudin-10* morphant embryos: 32% had reduced ($n=8/31$) or absent ($n=2/31$) *Snail1* expression in the right lateral plate mesoderm, and 16% of the embryos expressed *Snail1* bilaterally in the lateral plate mesoderm ($n=5/31$) (Fig. 3P–R). Surprisingly, genes expressed asymmetrically in the midline and left lateral plate mesoderm were also aberrantly expressed in the *Claudin-10* morphant embryos. Expression of *Lefty1* in the midline was absent in 60% ($n=6/10$) of the morphant embryos (Fig. 3E). *Nodal* expression was absent in the left lateral plate mesoderm of 29% ($n=4/14$) (Fig. 3B) and *Lefty2* expression was absent in 56% ($n=5/9$) of the morphant embryos (Fig. 3H). In contrast to the gain-of-function embryos, which exhibited randomized *Pitx2c* expression in the left lateral plate mesoderm, *Claudin-10* morphants exhibited right-sided *Pitx2c* expression ($n=2/13$) and bilateral *Pitx2c* expression ($n=1/13$) (Fig. 3K), suggesting that blocking Claudin-10 expression permits expression of *Pitx2c* on the right side. Interestingly, neither *Nodal* nor *Lefty2* were expressed on the right side in *Claudin-10* morphants. These data are summarized in Table 2.

These data place Claudin-10 functionally downstream of the events that generate asymmetric expression of *Shh* and *Fgf8* at Hensen's node and *Nodal* in the perinodal region, and upstream of evolutionarily-conserved asymmetric gene expression in the midline and lateral plate mesoderm. Furthermore, they support a role for Claudin-10 during the transfer of laterality cues between Hensen's node and the lateral plate mesoderm.

Residues in the first extracellular loop and cytoplasmic tail are critical for Claudin-10 function in left–right patterning

In vitro studies have been instrumental in defining claudin functional domains. Charged residues in the claudin first extracellular loop are important for determining the charge and size selectivity of the tight junction. Phosphorylation of residues in the cytoplasmic C-terminal tail is known to be important for claudin polymerization and stability, and can also influence the paracellular barrier properties of tight junctions (Raleigh et al., 2011; Van Itallie et al., 2012). The C-terminus also contains a PDZ-binding domain that is required for interactions with cytoplasmic adaptor proteins. Given the importance of these domains, we performed site-directed mutagenesis analysis of specific amino acid residues in the first extracellular loop and C-terminal cytoplasmic domain of Claudin-10 to determine if they were required for its left–right patterning activity (Fig. 4A).

The first extracellular loop of Claudin-10 contains seven charged residues that influence permeability of ions through the paracellular space. We used site-directed mutagenesis to mutate aspartic acid (D) residues D36, D56, D65, and D73 to positively charged lysines (K) to assess the contribution of paracellular permeability to the function of Claudin-10 in left–right patterning. We first characterized the effect of these mutations on Claudin-10 function in cell culture. All variants localized correctly to the tight junction in transiently transfected MDCK II cells (Fig. 4B). To determine if these mutations altered tight junction barrier properties, two standard assays to detect changes in paracellular permeability were performed: measurement of transepithelial resistance (TER) was used to assess changes in ion selectivity, and flux of a fluorescently-labelled dextran tracer through the paracellular space was used to assess changes in size permeability (reviewed in Tang and Goodenough, 2003). TER was measured in MDCK II monolayers transfected with wildtype Claudin-10 or the Claudin-10 variants (Fig. 4C). Transfection of wildtype Claudin-10 increased the TER 1.3-fold compared to the mock-transfected cells, suggesting an increase in barrier property. The D36K, D56K, D65K, and D73K charge-reversal mutations in the first extracellular loop lowered the TER to levels that were similar to mock transfected

Table 1
Effect of Claudin-10 gain-of-function on asymmetric gene expression.

Gene	RCAS-GFP		RCAS-Claudin-10			
	Left	Right	Left	Right	Bilateral	Absent
Nodal	100% ($n=10/10$)		60.0% ($n=6/10$)			40.0.% ($n=4/10$)
Lefty1	100% ($n=8/8$)		70.0% ($n=7/10$)			30.0% ($n=3/10$)
Lefty2	100% ($n=9/9$)		57.1% ($n=4/7$)			42.9% ($n=3/7$)
Pitx2c	100% ($n=17/17$)		83.3% ($n=30/36$)	8.3% ($n=3/36$)	5.6% ($n=2/36$)	2.8% ($n=1/36$)
Snail1		100% ($n=10/10$)		100% ($n=10/10$)		

Table 2
Effect Claudin-10 loss-of-function on asymmetric gene expression.

Gene	Mismatch MO			Claudin-10 MO				
	Left	Right	Reduced	Left	Right	Bilateral	Absent	Reduced
Nodal	100% ($n=10/10$)			71.4% ($n=10/14$)			28.6% ($n=4/14$)	
Lefty1	100% ($n=7/7$)			40.0% ($n=4/10$)			60.0% ($n=6/10$)	
Lefty2	100% ($n=7/7$)			44.4% ($n=4/9$)			55.6% ($n=5/9$)	
Pitx2c	100% ($n=14/14$)			76.9% ($n=10/13$)	15.4% ($n=2/13$)	7.8% ($n=1/13$)		
Snail1		93.3% ($n=14/15$)	6.7% ($n=1/15$)		51.6% ($n=16/31$)	16.1% ($n=5/31$)	6.5% ($n=2/31$)	25.8% ($n=8/31$)

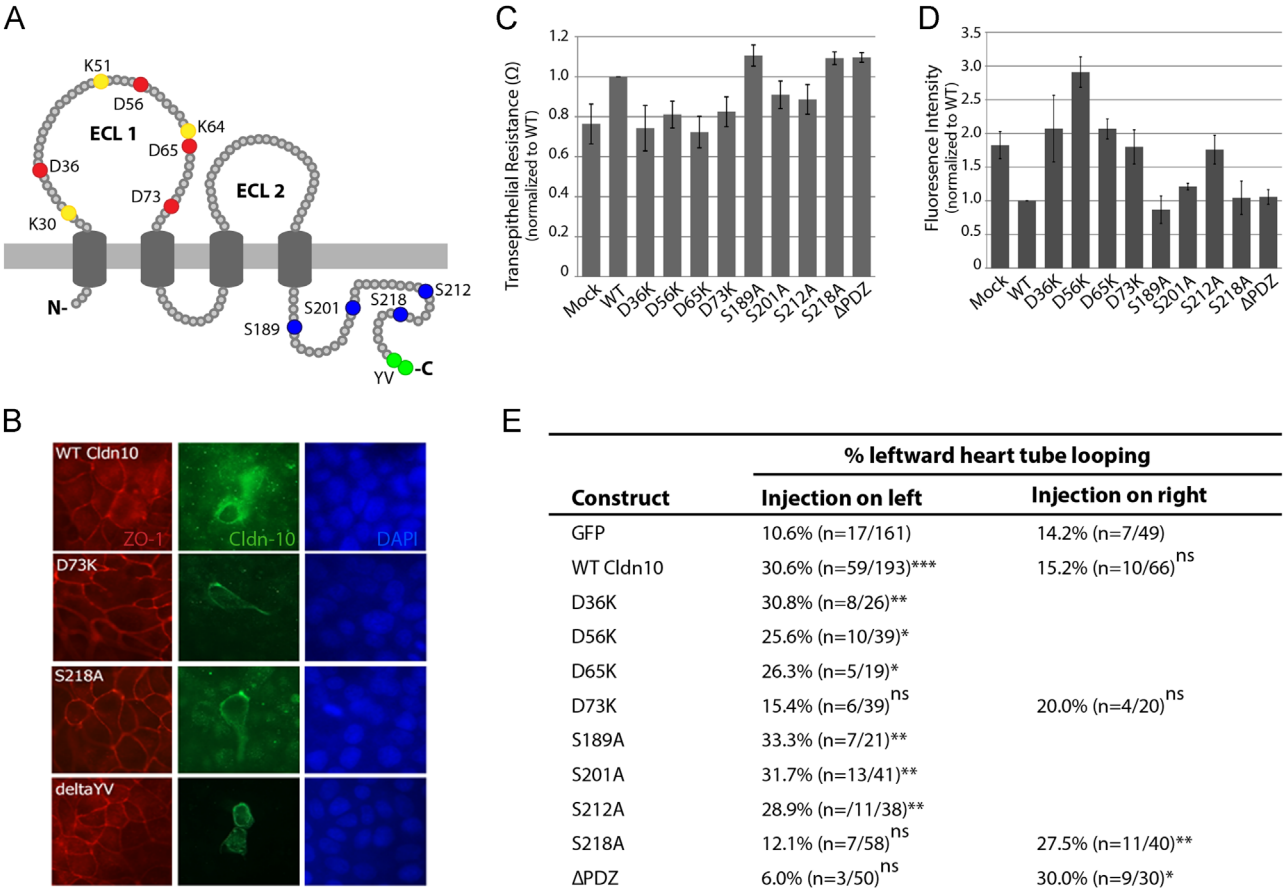

E

Construct	% leftward heart tube looping	
	Injection on left	Injection on right
GFP	10.6% (n=17/161)	14.2% (n=7/49)
WT Cldn10	30.6% (n=59/193)***	15.2% (n=10/66)^{ns}
D36K	30.8% (n=8/26)**	
D56K	25.6% (n=10/39)*	
D65K	26.3% (n=5/19)*	
D73K	15.4% (n=6/39)^{ns}	20.0% (n=4/20)^{ns}
S189A	33.3% (n=7/21)**	
S201A	31.7% (n=13/41)**	
S212A	28.9% (n=/11/38)**	
S218A	12.1% (n=7/58)^{ns}	27.5% (n=11/40)**
ΔPDZ	6.0% (n=3/50)^{ns}	30.0% (n=9/30)*

Fig. 4. *D73, S218, and the PDZ-binding domain are critical for Claudin-10 function.* (A) Schematic of Claudin-10 indicating the residues that were mutated to evaluate functional domains. Positively charged (yellow) and negatively charged (red) residues in the first extracellular loop, predicted sites for phosphorylation in the C-terminal tail (blue) and the PDZ binding domain (green) are shown. (B) Claudin-10 variants (green) colocalized with the tight junction adaptor protein ZO-1 (red) at the cell membrane in transiently transfected MDCK II cells. (C) Transepithelial electrical resistance values of MDCK II cells transiently transfected with Claudin-10 variants. Values are normalized to cells transfected with wildtype (WT) Claudin-10. (D) Flux of 4 kDa dextrans in MDCK II cells transiently transfected with Claudin-10 variants. Fluorescent intensities were normalized to wildtype (WT) transfection. (E) Gain-of-function experiments were performed on either the left or right side of Hensen's node as indicated for each Claudin-10 variant construct. Scores for abnormal leftward heart looping are shown. ns=non-significant as compared to GFP control score on same side; $^{*}p<0.05$, $^{**}p<0.005$, $^{***}p<0.0001$ all compared to GFP control score on the same side.

MDCK II cells. Cells transfected with the D36K, D56K, D65K, and D73K Claudin-10 variants showed an increase in flux of the 4 kDa fluorescent dextran compared to cells transfected with wildtype Claudin-10 (Fig. 4D), but no changes in permeability to a 40 kDa dextran were observed (data not shown).

We then tested the ability of these Claudin-10 variants to affect heart tube looping in a gain-of-function approach by misexpressing retroviral particles on the left side of Hensen's node at HH4 (Fig. 4E). Misexpression of the charge-reversal D36K, D56K, and D65K variants randomized the direction of heart-tube looping similarly to wild type Claudin-10 (Fig. 4E). In contrast, the D73K mutant abrogated Claudin-10's ability to alter the direction of heart tube looping when misexpressed on the left-side of Hensen's node (15.4%, $n=6/39$, $\chi^2=0.72$, $p=0.4$ compared to control GFP injection). These data suggest that D73 is important for Claudin-10 function in left–right patterning, while D36, D56 and D65 are not essential.

Table 3
S218A and ΔPDZ overexpression on the right affects asymmetric gene expression.

Gene	RCAS-ΔPDZ					RCAS-S218A			
	Left	Right	Bilateral	Absent	Reduced	Left	Right	Absent	Reduced
Nodal	77.7% ($n=14/18$)			22.2% ($n=4/18$)		75% ($n=12/16$)		25% ($n=4/16$)	
Snail1		37.5% ($n=3/8$)	12.5% ($n=1/8$)	12.5% ($n=1/8$)	37.5% ($n=3/8$)		50.0% ($n=4/8$)	25.0% ($n=2/8$)	25.0% ($n=2/8$)

We next created Claudin-10 variants with alterations in the cytoplasmic C-terminal tail, which contains phosphorylation sites and a PDZ-binding domain that mediates claudin interactions with adaptor proteins at the tight junction cytoplasmic plaque. Phosphorylation of residues in the C-terminal tail of claudins can influence the recruitment of claudins to the tight junction, stabilize interactions with scaffolding proteins, and change paracellular permeability properties (reviewed in Angelow et al., 2008; Hou et al., 2013). Using NetPhos 2.0 software (Blom et al., 1999) four putative phosphorylation sites were identified in the C-terminal tail of Claudin-10: S189, S201, S212, and S218. These sites were mutated to phosphorylation-null alanine (A) residues. To abolish the PDZ-binding domain, which is defined by the two terminal amino acids of the C-terminal tail (YV), a stop codon was inserted immediately prior to YV to generate the Claudin-10ΔPDZ variant. The phosphorylation-null variants (S189A, S201A, S212A, and S218A) and the ΔPDZ variant all localized to the tight junction in transfected MDCK II cells (Fig. 4B and data not shown). The S189A, S218A and ΔPDZ Claudin-10 variants increased the transepithelial resistance and decreased dextran flux of transfected MDCK II cells similarly to the effects of wildtype Claudin-10 (Fig. 4C and D and data not shown). In contrast, MDCK cells transfected with the S212A variant behaved similarly to mock transfected cells, suggesting that phosphorylation of S212 may influence paracellular permeability.

Next these variants were tested for their effect on Claudin-10 function with respect to left–right patterning. The S189A, S201A and S212A variants behaved similarly to wildtype Claudin-10 when they were misexpressed on the left side of Hensen's node at HH4: all increased the incidence of leftward looping of the heart tube (Fig. 4E). In contrast, misexpression of S218A or the ΔPDZ variant on the left side of Hensen's node did not increase the incidence of leftward heart tube looping above background (Fig. 4E). Thus, although S218 and the PDZ binding domain are not required for Claudin-10's paracellular barrier properties, they are essential for Claudin-10's function in the context of left–right patterning.

We then overexpressed the three variants that were unable to randomize heart looping in gain-of-function studies (D73K, S218A and ΔPDZ) on the right side of Hensen's node, where Claudin-10 is endogenously expressed. The D73K variant caused a small but insignificant increase in the incidence of leftward heart tube looping. In contrast, both S218A and ΔPDZ variants caused a significant increase in the incidence of leftward heart tube looping. Overexpression of the S218A variant on the right side of the embryo resulted in 27.5% abnormal leftward heart looping ($n=11/40$, $\chi^2=3.76$, $p<0.05$) in contrast to wildtype Claudin-10, which had no effect (15.2%, $n=10/66$). Similarly, overexpression of ΔPDZ on the right side of Hensen's node resulted in a 30% ($n=9/30$, $\chi^2=8.47$, $p<0.005$) incidence of leftward heart tube looping (Fig. 4E). Finally we examined the expression of *Nodal* and *Snail1* in these embryos. Expression of *Nodal* was absent from the left lateral plate mesoderm in 22% ($n=4/18$) of ΔPDZ-injected embryos and in 25% ($n=4/16$) of S218A-injected embryos (Table 3). *Snail1* expression was disrupted in 62.5% of embryos injected with ΔPDZ ($n=5/8$) and in 50% of embryos injected with S218A ($n=4/8$) (Table 3). Thus, the right-sided misexpression of the S218A or ΔPDZ variants had a similar effect on *Nodal* and *Snail1* expression to that observed in *Claudin-10* morphant embryos (Fig. 4A and B, Tables 1, 2), suggesting that these variants interfere with the function of endogenous wild-type Claudin-10.

Claudin-10 knockdown does not alter gross cell morphology at Hensen's node

Given the phenotypes observed using the Claudin-10 S218A and ΔPDZ variants, which are predicted to interact with the actin cytoskeleton and additional components at the cytoplasmic plaque, we tested whether cell morphology was disrupted at Hensen's node. To assess this, HH3-4 embryos were electroporated with *Claudin-10* MO or mismatch control MO and collected after 4 and 8 h. Cell shape and organization of actin filaments was evaluated by phalloidin staining and cell polarity was determined by Par-3 staining. No difference in cell shape or apical polarity was observed between control and Claudin-10 morphants at either time point (Supplemental Fig. 3).

Discussion

We previously determined that *Claudin-10*, an integral component of the tight junction, is asymmetrically expressed at Hensen's node (Collins et al., 2013). In this paper, we extended the temporal and spatial expression analysis and found that Claudin-10 localizes to tight junctions on the lateral surface of the right side of Hensen's node and in endodermal cells underlying Hensen's node. Claudin-10 expression must remain asymmetric for normal rightward heart looping: bilateral expression or knockdown of endogenous expression resulted in an increased incidence of abnormal leftward heart tube looping and disrupted expression of *Lefty1* in the midline, and *Nodal*, *Lefty2*, *Pitx2c*, and *Snail1* in the lateral plate mesoderm. We examined functional domains of Claudin-10 and identified that the first extracellular loop and the intracellular tail contain critical residues required for patterning the left–right axis. This study identifies a role for Claudin-10 at Hensen's node and suggests a novel function for tight junctions during the phase of left–right patterning when laterality cues are relayed from Hensen's node to the lateral plate mesoderm (Fig. 5).

Claudin-10 functions during transmission of laterality signals from Hensen's node to the lateral plate mesoderm

Patterning of the left–right axis can be broken down into distinct phases: symmetry-breaking events at the LRO that initiate the cascade, transmission of left–right information from the LRO to the lateral plate mesoderm, maintenance of left and right identity in the lateral plate mesoderm, and translation of this positional information to organ primordia. We have shown that Claudin-10 expression is restricted to the right side of Hensen's node between HH4 and HH7, which coincides with the establishment of

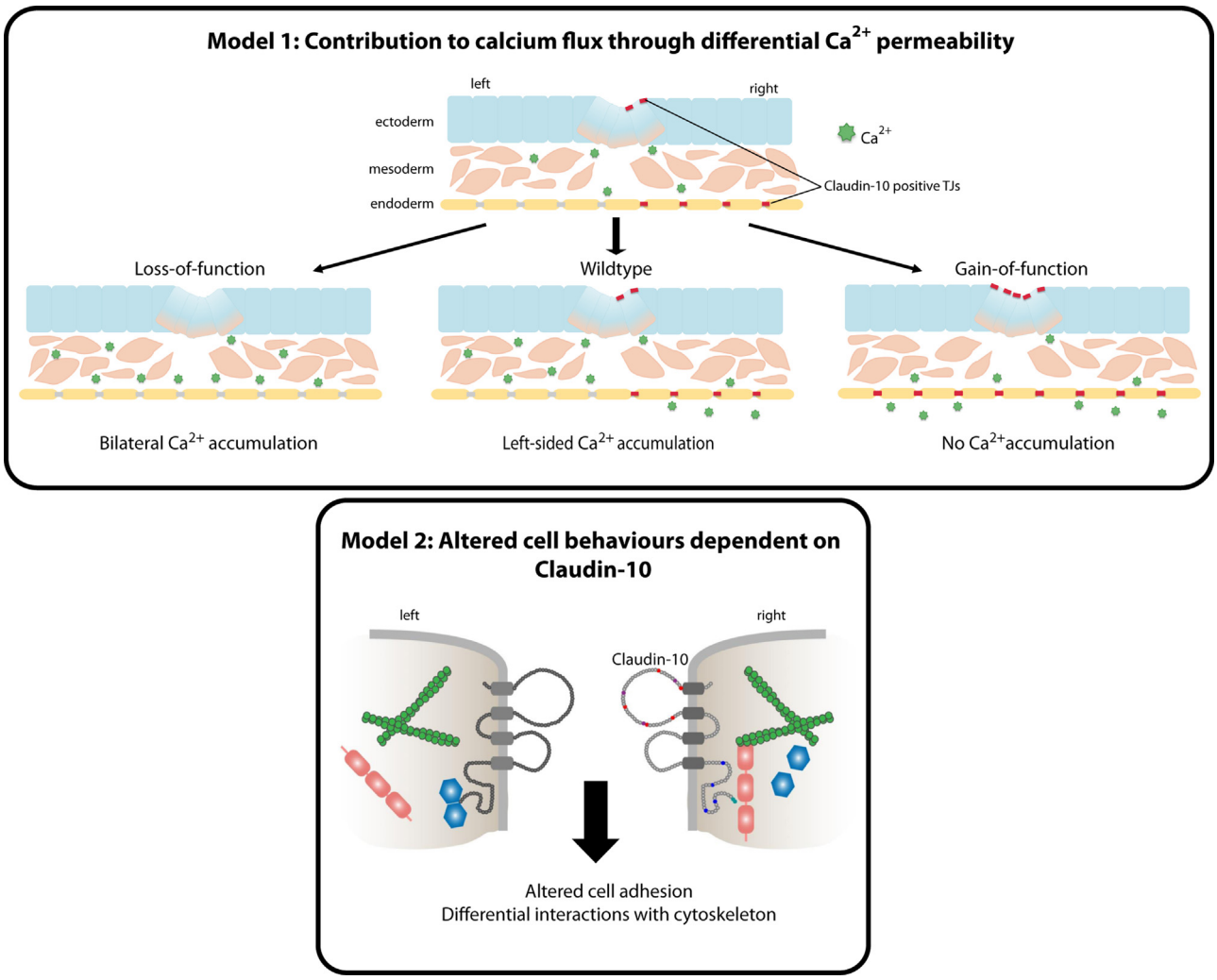

Fig. 5. Models for Claudin-10 function at Hensen's node. Model 1 outlines the contribution of Claudin-10 to the differential flux of calcium ions. Schematic of a transverse section through Hensen's node. Pink bars represent Claudin-10 positive tight junctions in the ectoderm and endoderm on the right side. Green stars represent extracellular calcium ions in the embryonic space. We propose a model where the presence of Claudin-10 in the endoderm on the right side prevents the accumulation of calcium ions that is required for downstream asymmetric gene expression. Model 2 outlines the hypothesis that Claudin-10 may differentially affect protein complex formation at the tight junction plaque to elicit altered cell behaviours between the left and right sides of the embryo.

asymmetry at Hensen's node and the period when left–right identity is transmitted to the lateral plate mesoderm. Retroviral misexpression of Claudin-10 on the left side randomized the direction of heart tube looping when the manipulation was performed at HH4 but not when the injections were performed at HH6. We generally observe a 4–6 h lag between retroviral particle injection and detection of retroviral mRNA. Incorporating this inherent delay in retroviral gene expression would mean that retroviral injection at HH4 would result in Claudin-10 expression at HH6, while embryos injected at HH6 would not express Claudin-10 bilaterally until late HH7. Thus, our gain-of-function data predict that Claudin-10 function is required between HH6 and HH7, which corresponds to the phase of left–right patterning when left versus right identity is propagated from Hensen's node to the lateral plate mesoderm. The ability of *Claudin-10* morpholinos to increase the incidence of heart tube looping when they are introduced at HH6 provides further evidence that Claudin-10 is required during the period that information is transferred from Hensen's node to the lateral plate mesoderm. Finally, the fact that manipulating *Claudin-10* expression did not affect left-sided *Shh* and right-sided *Fgf8* expression at Hensen's node, while asymmetric gene expression in the lateral plate mesoderm is altered in both the gain- and loss-of-function manipulations, temporally positions Claudin-10 function during the developmental window when left–right identity is being relayed from Hensen's node to the lateral plate mesoderm.

Claudin-10 is required for asymmetric gene expression in both left and right lateral plate mesoderm

Based on the spatially restricted domain in which Claudin-10 is expressed and its temporal requirement during left–right patterning, we hypothesize that Claudin-10 functions to transmit a signal that promotes right and/or inhibits left identity. Following this hypothesis, one would predict that knock-down of Claudin-10 expression would prevent expression of "right-identity" genes in the right lateral plate mesoderm and that ectopic expression of Claudin-10 on the left side would inhibit the expression of "left-identity" genes and/or induce the expression of "right-identity" genes in the left lateral plate mesoderm. Indeed, misexpression of Claudin-10 on the left side of Hensen's node blocked the left-sided expression of *Lefty1* in the midline and *Nodal* and *Lefty2* in the left lateral plate mesoderm in approximately one-third of injected embryos. *Pitx2c* expression in the left lateral plate mesoderm was affected in half the number of embryos that had absent *Nodal* expression, suggesting that *Pitx2c* expression is randomized

downstream of absent Nodal signalling. Ectopic expression of Claudin-10 on the left did not induce *Snail1* expression in the left lateral plate mesoderm. However, morpholino knockdown of endogenous Claudin-10 led to reduced or absent *Snail1* expression in the right lateral plate mesoderm. Combined, these data support the hypothesis that Claudin-10 function is required on the right side of the embryo to promote right identity and inhibit left-sided gene expression.

However, other aspects of our expression analysis suggest that Claudin-10 is not simply a straightforward promoter of right identity and inhibitor of left identity. First, a proportion of *Claudin-10* morphant embryos expressed *Snail1* bilaterally, rather than predicted absence or reduction. Second, there was the surprising observation that Claudin-10 knockdown led to loss of asymmetric gene expression on the left side of the embryo, very similar to what is observed when perinodal *Nodal* expression is removed (Brennan et al., 2002). Finally, the *Claudin-10* morphants exhibited right-sided expression of *Pitx2c*, in addition to the predicted bilateral expression. We interpret this to mean that the absence of Claudin-10 at Hensen's node makes the right lateral plate mesoderm permissive to express genes that are normally expressed in the left lateral plate mesoderm. However, the absence of right-sided *Nodal* expression in manipulated embryos suggests that manipulating Claudin-10 expression disconnects the Nodal-Pitx2c signalling cassette. It is difficult to assess how frequently the manipulation of left–right patterning genes disconnects the Nodal-Pitx2c signalling cassette since most studies only report effects on the expression of one component. Our data suggest that right-sided expression of Claudin-10 is also required to promote normal asymmetric expression on the left side of the embryo downstream of perinodal Nodal signalling. To the best of our knowledge, Claudin-10 is the only asymmetrically expressed protein that has the potential to regulate both left and right identity. It is clear that our understanding of the molecular mechanisms that relay left–right information from LRO to the lateral plate mesoderm is far from complete.

Mechanisms of Claudin-10 function in asymmetric morphogenesis

Junctional communication between cells within epithelial layers is important for relaying patterning cues that direct morphogenesis. Claudins are essential for tight junction formation and the specific combination of claudin family members in a cell directly affect its paracellular barrier properties. In addition, the cytoplasmic tail, which is the most unique region of each family member, participates in protein interactions at the tight junction cytoplasmic plaque at the apical cell surface. These interactions connect the tight junction to the actin cytoskeleton and are predicted to have critical roles in morphogenesis. As described above, asymmetric expression of Claudin-10 on the right side of Hensen's node is essential for asymmetric gene expression in the lateral plate mesoderm and normal rightward looping of the heart tube. Previously we showed that overexpression of Claudin-1 on the right side of Hensen's node randomizes the direction of heart tube looping (Simard et al., 2006). The effect of Claudin-1 overexpression is most likely due its competition with endogenous Claudin-10 for integration into the tight junctions on the right side of Hensen's node. Claudin-1 is known to generate anion selective tight junctions that act as cation barriers, while tight junctions containing Claudin-10 are predicted to be cation permissive (Van Itallie et al., 2006). Thus, altering the composition of claudins within the tight junction by substituting Claudin-1 for Claudin-10 is likely to change the paracellular permeability properties at Hensen's node.

However, maintaining the ionic barrier properties of the tight junction is unlikely to be the only role for claudins in left–right patterning. Similarly to Claudin-1, Claudin-3 generates tight junctions that are anion selective and cation barriers (Milatz et al., 2010). Yet, unlike Claudin-1, overexpression of Claudin-3 on the right side of Hensen's node does not affect left–right patterning (Simard et al., 2006). Thus, it is also possible that Claudin-1 antagonizes Claudin-10 function by competing for interactions within the tight junction cytoplasmic plaque that affect recruitment of intracellular proteins and/or interactions with the actin cytoskeleton. Our data showing that Claudin-10 variants that abrogate either paracellular barrier properties or interactions between its C-terminal tail and the cytoplasmic plaque suggest that both of these functional domains are required for Claudin-10 function in left–right patterning. These mechanisms are discussed in more detail below.

Left–right patterning activity of Claudin-10's first extracellular loop: modulation of Ca^{2+} signalling at Hensen's node

The best understood function of claudins is their role in regulating paracellular permeability at tight junctions (reviewed in Angelow et al., 2008; Hou et al., 2013). Charged residues within the first extracellular loop determine the specific permeability properties that the claudin molecule imparts to the tight junction. We tested the importance of negatively-charged residues in Claudin-10's first extracellular loop. Individual conversion of each of the four aspartic acid residues in the first extracellular loop to lysine should have the same effect on the net charge of this domain. Indeed, all four single amino acid mutations eliminated Claudin-10's ability to increase TER and reduce dextran flux in transfected cells. Yet, only the D73K mutation abrogated the ability of Claudin-10 to induce leftward heart tube looping when misexpressed on the left side of the embryo. Thus, the D73K mutation may not solely result in a change in the net negative charge of the first extracellular loop, but additionally, may also be important for the trans-interactions with claudins in adjacent cells.

Comparative sequence analysis of chick Claudin-10 showed that it is most closely related to human and mouse Claudin-10 isoform b (Supplemental Fig. 4), which have a net negative charge in their first extracellular loop that increases permeability to divalent cations (Van Itallie et al., 2006). Chick Claudin-10 has the same net negative charge in its first extracellular loop, suggesting that Claudin-10 containing tight junctions will also have increased permeability to cations. This property is particularly relevant given the evolutionarily-conserved role of calcium in left–right patterning. In the chick, calcium pools appear bilaterally and then become enriched on the left side of Hensen's node at gastrulation. Both extracellular and intracellular calcium enrichment on the left side of Hensen's node have been shown to be required for correct left–right patterning (Raya et al., 2004; Garic-Stankovic et al., 2008). Tight junctions between cells of Hensen's node may play a role in maintaining these extracellular pools. Since chick Claudin-10 is predicted to form a cation pore, its expression on the right side would permit calcium ions to pass freely between cells thereby inhibiting an enrichment of calcium ions. Tight junctions on the left side, which lack Claudin-10, would be predicted to provide a cation barrier and consequently promote an accumulation of extracellular calcium on the left. Thus, asymmetric expression of Claudin-10 may have a significant role in generating the differential calcium gradient between the left and right sides of the embryo.

The effects on gene expression observed following manipulation of Claudin-10 expression fit this model. Misexpression of Claudin-10 on the left side should make the left side leakier to calcium and consequently prevent a left-sided calcium flux and the induction of asymmetric gene expression in the left lateral plate mesoderm. Knockdown of Claudin-10 on the right side

should make the right side tighter with respect to calcium movement through the paracellular space and consequently prevent formation of a differential calcium gradient between the left and right sides. Ultimately this would prevent a left-sided calcium enrichment and also block subsequent asymmetric expression of genes in the left lateral plate mesoderm. Additional experiments that assay the specific effects on calcium ion permeability are needed to confirm this hypothesis.

The Claudin-10 cytoplasmic tail is a critical functional domain for left–right identity

Claudin family members exhibit the greatest sequence diversity within their C-terminal tails, which interact with cytoplasmic scaffolding and adaptor proteins to form a signalling platform referred to as the tight junction cytoplasmic plaque. These interactions also link the tight junction to the actin cytoskeleton (Hartsock and Nelson, 2008). Claudin C-terminal tails are also subject to post-translational modifications, including phosphorylation (Findley and Koval, 2009). Thus, individual claudin family members are likely to participate in distinct multi-protein complexes at the cytoplasmic plaque, where these interactions have the potential to be regulated via post-translational modifications.

We have identified two important domains within the tail of Claudin-10 that are involved in its function in left–right patterning: S218 and the PDZ-binding domain residues YV at positions 227–228. In our gain-of-function experiments these mutants are unable to randomize the direction of heart tube looping when misexpressed on the left side of Hensen's node, suggesting that they are required for the effects on heart tube looping observed following overexpression of wild type Claudin-10. Also, overexpression of both the ΔPDZ and S218A variants on the right side disrupted *Nodal* and *Snail1* expression similarly to the loss-of-function manipulation. Neither of these variants changed Claudin-10's effect on TER and dextran flux suggesting that they do not impact Claudin-10's paracellular barrier properties. We hypothesize that these variants act as competitive inhibitors, such that they are able to compete for position within the tight junction network but unable to interact with proteins at the cytoplasmic plaque required to elicit the specific patterning activities of endogenous Claudin-10. The identification of protein interaction partners and examination of their specificity for individual claudin family members will be necessary to fully understand the effects of these variants.

Scaffolding proteins such as ZOs, PATJ, PALS1, and MUPP1, contain multiple PDZ repeats and are recruited to the tight junction via the PDZ-binding domain in the claudin C-terminal tails. Additionally, the stability of these interactions is affected by the phosphorylation status of residues within claudin tails. Phosphorylation of claudin tails has also been shown to be important for recruitment and localization of claudins to the tight junction, as well as enhancement or attenuation of barrier function. Although four phosphorylation sites were predicted in the Claudin-10 tail, only S218 proved to be an important for the role of Claudin-10 in left–right patterning. This residue is the closest predicted phosphorylation site to the PDZ-binding domain. Given the proximity to this interaction domain, differential phosphorylation of S218 residue may be important in modulating interactions between Claudin-10 and scaffolding proteins. Our analysis revealed that neither actin organization nor cell polarity at Hensen's node was affected in Claudin-10 morphant embryos, however, this does not eliminate the possibility that additional cytoplasmic plaque components may be aberrantly recruited to the tight junction, or that these residues may be important for the modulation of extracellular barrier properties. Thus, our data support the hypothesis that Claudin-10 may differentially affect protein complex formation at the tight junction cytoplasmic plaque that ultimately contributes to left–right differences in cell adhesion that may be required for the relay of information between Hensen's node and the lateral plate mesoderm. Indeed, this model is nicely supported by data from *Xenopus* in which overexpression of the claudin *Xcla* disrupted blastomere adhesion in animal cap assays, and overexpression in the embryo leads to randomized organ situs and *Nodal* expression (Brizuela et al., 2001).

Summary

In summary, our data demonstrate a unique and novel role for Claudin-10 in transmitting laterality information between Hensen's node and the lateral plate mesoderm. It is tempting to speculate that Claudin-10 is critical for generating a differential calcium signalling gradient between the left and right sides of the embryo that parallels the outcome of nodal flow in vertebrates where motile cilia are essential for left–right patterning. It is also interesting to consider the possibility that the cells expressing Claudin-10 on the lateral surface of the node have a function that is similar to the role described for the mouse endoderm in relaying left–right patterning cues from the LRO. Both of these cell populations are comparable with respect to their exposure to extracellular signals and connection to the LRO. In addition, Claudin-10 may asymmetrically regulate cell behaviours through its interactions with adaptor proteins and the actin cytoskeleton at the tight junction cytoplasmic plaque. Further studies are needed to define if Claudin-10's function is evolutionarily conserved and/or identify parallel molecular mechanisms in other species.

Materials and methods

Embryo collection and whole-mount in situ hybridization

Fertilized eggs (Couvoir Simentin, Mirabel, Quebec) were incubated at 39 °C until the correct stages were reached. Embryos were staged according to Hamburger and Hamilton staging criteria (Hamburger and Hamilton, 1951). Dissected embryos were collected in DEPC-PBS and fixed overnight in 4% paraformaldehyde in PBS. Whole-mount *in situ* hybridization was performed as previously described (Collins and Ryan, 2011). Full-length *Claudin-10* cDNA (Accession XM_001232226.2) was cloned from HH4 mRNA using the OneStep RT-PCR kit (QIAGEN) into the pSC-A plasmid using the StrataClone™ PCR Cloning kit (Stratagene) and sequenced to confirm correct sequence and orientation. DIG-labelled riboprobes against *Claudin-10* were generated by linearizing the pSC-Claudin-10 vector with BamHI and transcribed using T3 polymerase. *Shh*, *Fgf8*, *Nodal*, *Lefty*, *Pitx2c*, and *Snail* probes were synthesized as previously described (Simard et al., 2006).

Protein expression

Embryos were fixed in 10% trichloroacetic acid for 30 min on ice and rinsed in PBS. Tissue was cryoprotected in sucrose and embedded in Tissue Tek OCT compound. Blocks were sectioned at 10 μm and collected on Fisherbrand Superfrost Plus microscope slides. For immunohistochemistry on sections, rabbit anti-Claudin-10 (Invitrogen) and mouse anti-ZO-1 (Invitrogen) were used at 1:100 dilution, and detected using Alexa Fluor 488 conjugated goat anti-rabbit IgG or Alexa Fluor 594 conjugated goat anti-mouse IgG (Invitrogen) at 1:500 dilution. Mouse anti-Par-3 (Millipore) was used at 1:250 and detected by Alexa Fluor 594 conjugated goat anti-mouse IgG (Invitrogen) at 1:500 dilution. Phalloidin (Invitrogen) staining was performed in a 1:50 dilution. Slides were coverslipped with SlowFade® Light Antifade kit (Invitrogen). For whole-mount immunohistochemistry, embryos were incubated in 1:50 dilution of primary antibodies and a 1:250

dilution of secondary antibodies. Embryos and sections were imaged on a Zeiss laser scanning microscope LSM 780.

Protein was extracted from whole HH12 embryos electroporated with Claudin-10 or mismatch control morpholino. Total protein extract was separated by SDS-PAGE and transferred to a nitrocellulose membrane. Membranes were incubated with rabbit anti-Claudin-10 or anti-Claudin-1 antibodies (Invitrogen) at 1:500. Detection was performed using the ECL Western Blot Detection System (Amersham).

Claudin-10 knockdown

Morpholino antisense oligonucleotides (MOs) were designed by Gene Tools (Philomath, OR) against the translation start site of *Claudin-10* and tagged with fluorescein. Control experiments were performed using a 5 base pair mismatch MO. Sequences for MOs are shown in the 5′–3′ directions with the start site underlined, mismatch nucleotides are shown in lower case, and the corresponding nucleotide positions indicated.

Claudin-10 MO: GATCTCCGCCGACGTGCTCGCCATC; nucleotides −1 to +24.

Claudin-10 5 bp Mismatch MO: GATCTgCcCCGACcTGgTCcCCATC; nucleotides −1 to +24.

Morpholinos were stored at room temperature at 3 mM and diluted to 1 mM in sterile water, 0.6 μM sucrose, and with 0.1 μg/μl empty vector DNA (pBKS) as previously described (Voiculescu et al., 2008). For manipulations, embryos were collected at HH3-4$^-$ on filter paper supports and cultured *ex ovo* on agar albumin plates as previously described (Chapman et al., 2001; Collins and Ryan, 2011). Following MO injection at Hensen's node, embryos on the filter paper support were moved to an electroporation chamber with Tyrode's solution above and below the embryo, and electroporated using a CUY21SC Square Wave electroporator (Protech International, Boerne, Texas) under the following conditions: 2 pulses of 3 V, 50 ms pulse length at 1 s intervals. Once electroporated, embryos were moved back to the agar albumin plate, cultured in a humidified incubator at 39 °C for 24–36 h, and scored for the direction of heart tube looping.

Retroviral overexpression of Claudin-10

Full-length *Claudin-10* sequence was subcloned from pSC-A Claudin-10 into Slax and subsequently, the RCAS (B) plasmid. Retroviral particles were generated as previously described (Collins and Ryan, 2011). Briefly, RCAS-Claudin-10 was transfected into chick DF1 cells using Lipofectamine 2000 (Invitrogen). Transfected cells were expanded in culture to confluency. To collect viral particles, media was changed to 2% FBS in DMEM without antibiotics. Media was collected after 24 h for three days, filtered through a 0.45 μm sterile cellulose acetate filter and centrifuged at 4 °C for 3 h at 22,000 rpm in SW28 swinging bucket rotor without the brake. Viral pellets were resuspended in a minimum volume of DMEM, aliquoted and stored at −80 °C. Embryos were collected on filter paper supports and cultured *ex ovo* on agar albumin plates (Chapman et al., 2001; Collins and Ryan, 2011). Viral particles were injected on either the right or left side of Hensen's node using a Narishige IM 300 microinjector. Manipulated embryos were cultured for 24–36 h and scored for the direction of heart tube looping.

Generation of Claudin-10 mutant constructs

Predicted phosphorylation sites in the C-terminal tail of Claudin-10 were identified using NetPhos 2.0 (Blom et al., 1999) and mutated to phosphorylation-null alanine residues at positions S189, S201, S212, and S218. The PDZ-binding domain was removed by inserting a premature stop codon immediately upstream of the YV, the terminal two amino acids. For extracellular loop mutants, positive and negative residues were identified and compared with known important residues for ion permeability already investigated in the mouse (Van Itallie et al., 2006). Site-directed mutagenesis was performed using the Stratagene QuikChange Site-Directed Mutagenesis kit according to manufacturer's directions. Clones were sequenced to confirm their identity. Mutant constructs were then cloned into the RCAS (B) vector and retroviral particles were generated as described above. Sequences of mutagenesis primers are shown below.

Cldn10mu-tATG-5′	gccgacccatatggcatc-cacgtcggcggag
Cldn10mu-tATG-3′	ccgacccatatggcatccac-gagcgccga-gatcgtcgccttcctgc
Cldn10ΔY-V-5′	gacaagaacgcttgatcataagct-tatcgatacc
Cldn10ΔY-V-3′	ggtatcgataagcttatgat-caagcgttcttgtc
Cldn10-S189A-5′	cttctcgatagctgagaacag-taaagagccaaggagagcgtatg-catat
Cldn10-S189A-3′	atatgca-tacgctctccttggctctt-tactgttctcagctatcgagaag
Cldn10-S201A-5′	catataatggagccgcagctgt-gatgtcgtctcgt
Cldn10-S201A-3′	acgagacgacatca-cagctgcggctccattatatg
Cldn10-S212A-5′	ctcgtacaaagattca-caacgctgtcccagacaaaacct-cac
Cldn10-S212A-3′	gtgaggttttgtctggga-cagcgttgtgaatctttgtacgag
Cldn10-S218A-5′	gtgtcccagacaaaaccgcac-caaagcactttgac
Cldn10-S218A-3′	gtcaaagtgctttggtgcggtttt-gtctgggacac
Cldn10-D36K-5′	gaaggtgtcttccatcaaggg-cacggtcatcacca
Cldn10-D36K-3′	tggtgatgaccgtgcccttgatg-gaagacaccttc
Cldn10-D56K-5′	gacctgcgtgaccaagtc-caccggcgtct
Cldn10-D56K-3′	agacgccggtggacttggtcacg-caggtc
Cldn10-D65K-5′	cgtctccaactgcaa-gaagttcccgtccatgctgg
Cldn10-D65K-3′	ccagcatggacgggaacttcttg-cagttggagacg
Cldn10-D73K-5′	gtccatgctggctctcaagggtta-catccaagcct
Cldn10-D73K-3′	aggcttggatgtaacccttga-gagccagcatggac

Measuring transepithelial electrical resistance and dextran flux in MDCK monolayers

MDCK II cells were seeded in 24-well plates with 6.5 mm Transwell inserts with 0.4 μm pores (Corning). Cells were transfected with pcDNA3.1 plasmids containing Claudin-10 variants using Lipofectamine 2000 (Invitrogen) according to manufacturer's instructions. After 24 h, transepithelial electrical resistance (TER) was measured across confluent monolayers using a EVOM^2

voltohmmeter with STX2 electrodes (World Precision Instruments). Experimental manipulations were performed in triplicate per plate and repeated in three independent transfections. TER values were normalized to surface area of the insert. Monolayers were subsequently incubated with 0.05 mg/ml of 4 kDa and 40 kDa fluorescently-labelled dextrans (Sigma) in the upper chamber for 3 h. Dextran flux was measured by quantifying the amount of fluorescence detected in the lower chamber using a VICTOR X Multilabel plate reader (Perkin-Elmer). Each well was measured in triplicate and experiment was performed in at least three biological replicates. Dextran flux values were normalized to the mock transfected cells.

Acknowledgements

We would like to thank members of the Ryan lab, I. Gupta, and L. Jerome-Majewska for helpful discussions and comments. MMC is the recipient of a doctoral studentship from the Fonds de la Recherche en Santé du Quebec (FRSQ). This work was supported by a Natural Sciences and Engineering Research Council of Canada Discovery Grant (234319) and Canadian Institutes of Health Research Operating Grant (MOP-84583)to AKR. AKR is a member of the Research Institute of the McGill University Health Centre, which is supported in part by the FRSQ.

Appendix A. Supporting information

Supplementary data associated with this article can be found in the online version at http://dx.doi.org/10.1016/j.ydbio.2015.02.019.

References

Adams, D.S., Robinson, K.R., Fukumoto, T., Yuan, S., Albertson, R.C., Yelick, P., Kuo, L., McSweeney, M., Levin, M., 2006. Early, H+-V-ATPase-dependent proton flux is necessary for consistent left–right patterning of non-mammalian vertebrates. Development 133, 1657–1671.

Angelow, S., Ahlstrom, R., Yu, A.S., 2008. Biology of claudins. Am. J. Physiol. Ren. Physiol. 295, F867–876.

Aw, S., Adams, D.S., Qiu, D., Levin, M., 2008. H, K-ATPase protein localization and Kir4.1 function reveal concordance of three axes during early determination of left–right asymmetry. Mech. Dev. 125, 353–372.

Aw, S., Koster, J.C., Pearson, W., Nichols, C.G., Shi, N.Q., Carneiro, K., Levin, M., 2010. The ATP-sensitive K(+)-channel (K(ATP)) controls early left–right patterning in Xenopus and chick embryos. Dev. Biol. 346, 39–53.

Blom, N., Gammeltoft, S., Brunak, S., 1999. Sequence and structure-based prediction of eukaryotic protein phosphorylation sites. J. Mol. Biol. 294, 1351–1362.

Boettger, T., Wittler, L., Kessel, M., 1999. FGF8 functions in the specification of the right body side of the chick. Curr. Biol. 9, 277–280.

Brennan, J., Norris, D.P., Robertson, E.J., 2002. Nodal activity in the node governs left–right asymmetry. Genes Dev. 16, 2339–2344.

Brizuela, B.J., Wessely, O., De Robertis, E.M., 2001. Overexpression of the Xenopus tight-junction protein claudin causes randomization of the left–right body axis. Dev. Biol. 230, 217–229.

Chapman, S.C., Collignon, J., Schoenwolf, G.C., Lumsden, A., 2001. Improved method for chick whole-embryo culture using a filter paper carrier. Dev Dyn 220, 284–289.

Collins, M.M., Ryan, A.K., 2011. Manipulating claudin expression in avian embryos. Methods Mol. Biol. 762, 195–212.

Collins, M.M., Baumholtz, A.I., Ryan, A.K., 2013. Claudin family members exhibit unique temporal and spatial expression boundaries in the chick embryo. Tissue Barriers 1, e24517.

Cui, C., Little, C.D., Rongish, B.J., 2009. Rotation of organizer tissue contributes to left–right asymmetry. Anat. Rec. 292, 557–561.

Findley, M.K., Koval, M., 2009. Regulation and roles for claudin-family tight junction proteins. IUBMB Life 61, 431–437.

Fukumoto, T., Blakely, R., Levin, M., 2005a. Serotonin transporter function is an early step in left–right patterning in chick and frog embryos. Dev. Neurosci. 27, 349–363.

Fukumoto, T., Kema, I.P., Levin, M., 2005b. Serotonin signaling is a very early step in patterning of the left–right axis in chick and frog embryos. Curr. Biol. 15, 794–803.

Furuse, M., Hata, M., Furuse, K., Yoshida, Y., Haratake, A., Sugitani, Y., Noda, T., Kubo, A., Tsukita, S., 2002. Claudin-based tight junctions are crucial for the mammalian epidermal barrier: a lesson from claudin-1-deficient mice. J. Cell Biol. 156, 1099–1111.

Garic-Stankovic, A., Hernandez, M., Flentke, G.R., Zile, M.H., Smith, S.M., 2008. A ryanodine receptor-dependent Ca(i)(2+) asymmetry at Hensen's node mediates avian lateral identity. Development 135, 3271–3280.

Gonzalez-Mariscal, L., Betanzos, A., Nava, P., Jaramillo, B.E., 2003. Tight junction proteins. Prog. Biophys. Mol. Biol. 81, 1–44.

Grande, C., 2010. Left-right asymmetries in Spiralia. Integr. Comp. Biol. 50, 744–755.

Grande, C., Patel, N.H., 2009. Lophotrochozoa get into the game: the nodal pathway and left/right asymmetry in bilateria. Cold Spring Harb. Symp. Quant. Biol. 74, 281–287.

Gros, J., Feistel, K., Viebahn, C., Blum, M., Tabin, C.J., 2009. Cell movements at Hensen's node establish left/right asymmetric gene expression in the chick. Science 324, 941–944.

Gupta, I.R., Ryan, A.K., 2010. Claudins: unlocking the code to tight junction function during embryogenesis and in disease. Clin. Genet. 77, 314–325.

Hamburger, V., Hamilton, H.L., 1951. A Series of normal stages in the development of the chick embryo. J. Morphol. 88, 49.

Hartsock, A., Nelson, W.J., 2008. Adherens and tight junctions: structure, function and connections to the actin cytoskeleton. Biochim. Biophys. Acta 1778, 660–669.

Hou, J., Rajagopal, M., Yu, A.S., 2013. Claudins and the kidney. Annu. Rev. Physiol. 75, 479–501.

Katsu, K., Tatsumi, N., Niki, D., Yamamura, K., Yokouchi, Y., 2013. Multi-modal effects of BMP signaling on Nodal expression in the lateral plate mesoderm during left–right axis formation in the chick embryo. Dev. Biol. 374, 71–84.

Katsu, K., Tokumori, D., Tatsumi, N., Suzuki, A., Yokouchi, Y., 2012. BMP inhibition by DAN in Hensen's node is a critical step for the establishment of left–right asymmetry in the chick embryo. Dev. Biol. 363, 15–26.

Levin, M., Mercola, M., 1998. Gap junctions are involved in early determination of left–right asymmetry. Dev. Biol. 198 160-160.

Luo, Y.J., Su, Y.H., 2012. Opposing nodal and BMP signals regulate left–right asymmetry in the sea urchin larva. PLoS Biol. 10, e1001402.

Milatz, S., Krug, S.M., Rosenthal, R., Gunzel, D., Muller, D., Schulzke, J.D., Amasheh, S., Fromm, M., 2010. Claudin-3 acts as a sealing component of the tight junction for ions of either charge and uncharged solutes. Biochim. Biophys. Acta 1798, 2048–2057.

Nakamura, T., Hamada, H., 2012. Left-right patterning: conserved and divergent mechanisms. Development 139, 3257–3262.

Okumura, T., Utsuno, H., Kuroda, J., Gittenberger, E., Asami, T., Matsuno, K., 2008. The development and evolution of left–right asymmetry in invertebrates: lessons from Drosophila and snails. Dev. Dyn. 237, 3497–3515.

Raleigh, D.R., Boe, D.M., Yu, D., Weber, C.R., Marchiando, A.M., Bradford, E.M., Wang, Y., Wu, L., Schneeberger, E.E., Shen, L., Turner, J.R., 2011. Occludin S408 phosphorylation regulates tight junction protein interactions and barrier function. J. Cell Biol. 193, 565–582.

Raya, A., Kawakami, Y., Rodriguez-Esteban, C., Ibanes, M., Rasskin-Gutman, D., Rodriguez-Leon, J., Buscher, D., Feijo, J.A., Izpisua Belmonte, J.C., 2004. Notch activity acts as a sensor for extracellular calcium during vertebrate left–right determination. Nature 427, 121–128.

Saund, R.S., Kanai-Azuma, M., Kanai, Y., Kim, I., Lucero, M.T., Saijoh, Y., 2012. Gut endoderm is involved in the transfer of left–right asymmetry from the node to the lateral plate mesoderm in the mouse embryo. Development 139, 2426–2435.

Shen, M.M., 2007. Nodal signaling: developmental roles and regulation. Development 134, 1023–1034.

Simard, A., Di Pietro, E., Young, C.R., Plaza, S., Ryan, A.K., 2006. Alterations in heart looping induced by overexpression of the tight junction protein Claudin-1 are dependent on its C-terminal cytoplasmic tail. Mech. Dev. 123, 210–227.

Steed, E., Balda, M.S., Matter, K., 2010. Dynamics and functions of tight junctions. Trends Cell Biol. 20, 142–149.

Tang, V.W., Goodenough, D.A., 2003. Paracellular ion channel at the tight junction. Biophys. J. 84, 1660–1673.

Van Itallie, C.M., Tietgens, A.J., LoGrande, K., Aponte, A., Gucek, M., Anderson, J.M., 2012. Phosphorylation of claudin-2 on serine 208 promotes membrane retention and reduces trafficking to lysosomes. J. Cell Sci. 125, 4902–4912.

Van Itallie, C.M., Rogan, S., Yu, A., Vidal, L.S., Holmes, J., Anderson, J.M., 2006. Two splice variants of claudin-10 in the kidney create paracellular pores with different ion selectivities. Am. J. Physiol. Ren. Physiol. 291, F1288–1299.

Vanhoven, M.K., Bauer Huang, S.L., Albin, S.D., Bargmann, C.I., 2006. The claudin superfamily protein nsy-4 biases lateral signaling to generate left–right asymmetry in C. elegans olfactory neurons. Neuron 51, 291–302.

Viotti, M., Niu, L., Shi, S.H., Hadjantonakis, A.K., 2012. Role of the gut endoderm in relaying left–right patterning in mice. PLoS Biol. 10, e1001276.

Voiculescu, O., Papanayotou, C., Stern, C.D., 2008. Spatially and temporally controlled electroporation of early chick embryos. Nat. Protoc. 3, 419–426.

Yu, X., St_Amand, T.R., Wang, S., Li, G., Zhang, Y., Hu, Y.P., Nguyen, L., Qiu, M.S., Chen, YP., 2001. Differential expression and functional analysis of Pitx2 isoforms in regulation of heart looping in the chick. Development 128, 1005–1013.